Switched Tracking Control of the Lower Limb During Asynchronous Neuromuscular Electrical Stimulation: Theory and Experiments

Ryan J. Downey, Teng-Hu Cheng, Matthew J. Bellman, and Warren E. Dixon, *Fellow, IEEE*

***Abstract*—Neuromuscular electrical stimulation (NMES) induces muscle contractions via electrical stimuli. NMES can be used for rehabilitation and to enable functional movements; however, a fundamental limitation is the early onset of fatigue. Asynchronous stimulation is a method that can reduce fatigue by utilizing multiple stimulation channels to segregate and switch between different sets of recruited motor units. However, switching between stimulation channels is challenging due to each channel's differing response to stimulation. To address this challenge, a switched systems analysis is used in the present work to design a controller that allows for instantaneous switching between stimulation channels. The developed controller yields semi-global exponential tracking of a desired angular trajectory for a person's knee-joint. Experiments were conducted in six able-bodied individuals. Compared to conventional stimulation, the results indicate that asynchronous stimulation with the developed controller yields longer durations of successful tracking despite different responses between the stimulation channels.**

***Index Terms*—Asynchronous stimulation, fatigue, functional electrical stimulation (FES), neuromuscular electrical stimulation (NMES), nonlinear control, switched systems.**

I. INTRODUCTION

NEUROMUSCULAR electrical stimulation (NMES) induces muscle contractions by applying electrical stimuli and has been shown to be a useful rehabilitative treatment (e.g., in spinal cord injury [1], stroke [2], and cerebral palsy [3]). Beyond rehabilitation, NMES can be also used to enable functional movements (e.g., cycling [4], [5], grasping [6], reaching [7], and walking [8]), where it is termed functional electrical stimulation (FES). While the health benefits of NMES and its potential to restore functional movements are enticing, the early onset and rapid rate of fatigue during electrical stimulation limits its use in both applications. One suggested cause of fatigue is that conventional, single-channel stimulation is nonselective, spatially fixed, and temporally synchronous [9], [10], in contrast to the activation pattern of volitional contractions. To counteract this suggested cause of fatigue, researchers have developed asynchronous stimulation [11]–[29] as an alternative to conventional stimulation.

Asynchronous stimulation uses multiple stimulation channels with multiple spatially distributed electrodes to segregate the muscle group (or single muscle) of interest into multiple sets of muscles (or motor units). Electrical stimuli are then delivered as interleaved low frequency pulse trains. In other words, the pulse trains for each channel are phase shifted with respect to each other, thereby only activating one stimulation channel at any given time. By interleaving the pulses, a higher composite stimulation frequency can be achieved while maintaining low frequency stimulation in each channel to reduce fatigue. For example, four-channel asynchronous stimulation with 16 Hz yields a composite stimulation frequency equivalent 64 Hz single-channel stimulation, but, assuming there is no activation overlap, the motor units recruited by each stimulation channel are only activated at 16 Hz, and therefore, fatigue at a rate similar to 16 Hz conventional stimulation.

While asynchronous stimulation has been shown to reduce fatigue in open-loop experiments (see [13], [15], [16], [18]–[26], [28], [29]), the method presents challenges for closed-loop control. Specifically, because electrical stimuli are switched between multiple stimulation channels with spatially distributed electrodes, each stimulation channel is likely to recruit different motor units (with potential for activation overlap). Therefore, the evoked muscle force is expected to be different for each stimulation channel, even if each channel receives a stimulus with the same exact parameters (i.e., pulse amplitude and width). Therefore, switching between stimulation channels yields discontinuities in the torque produced about the knee-joint. Such discontinuities can lead to undesirable limb motions that may inhibit functional rehabilitation treatments. Thus, to develop feedback-based methods for FES that can take advantage of the potential benefits of switched, asynchronous stimulation, new control development, and justifying stability analysis is motivated.

While constructive control developments and associated stability analyses have been previously developed for

Manuscript received September 7, 2015; revised March 9, 2016; accepted March 11, 2016. Date of publication April 4, 2016; date of current version April 13, 2017. This work was supported by the National Science Foundation under Award 1161260. This paper was recommended by Associate Editor Z.-G. Hou.

R. J. Downey was with the University of Florida, Gainesville, FL 32611-6250 USA. He is now with the College of Health Professions, Medical University of South Carolina, Charleston, SC 29425 USA (e-mail: downeyr@musc.edu).

T.-H. Cheng, M. J. Bellman, and W. E. Dixon are with the Department of Mechanical and Aerospace Engineering, University of Florida, Gainesville, FL 32611-6250 USA (e-mail: tenghu@ufl.edu; mattjo@ufl.edu; wdixon@ufl.edu).

Color versions of one or more of the figures in this paper are available online at http://ieeexplore.ieee.org.

Digital Object Identifier 10.1109/TCYB.2016.2543699

conventional single-channel stimulation [4], [30]–[35], limited development has been provided for multichannel asynchronous stimulation. Lau *et al.* [27] studied standing in cats and found that the duration of standing achieved during closed-loop control of asynchronous stimulation was longer than that for open-loop control. However, the closed-loop controller implemented was a logic-based if-then-else algorithm without modeling or stability analysis. Similarly, Frankel *et al.* [36] implemented an iterative learning controller for isometric force control in cats; however, no modeling or stability analysis was included. Downey *et al.* [37] developed an robust integral of the sign of the error-based (RISE) control law for asynchronous stimulation that achieved semi-global asymptotic lower limb trajectory tracking. However, the control design required there to be a window of time where the control input is transitioned from one channel to another. Heuristically, a transition period is expected to lead to increased muscle fatigue since each stimulation channel will be activated longer than otherwise desired. Furthermore, in practice, stimulation channels are instantly switched, motivating the design of a control law that allows for instant switching. In [37], the transition period can be made arbitrarily small to approximate instant switching, but increased control gains are required to compensate for smaller transition periods. The previous work also implicitly assumes that the motor units recruited by each stimulation channel are independent. Yet, some degree of activation overlap is expected in practice, and therefore, it is motivated to remove this assumption in the control design.

Based on preliminary work in [38], a switched systems analysis is used to examine an alternative control approach that allows for instantaneous switching between stimulation channels, without additional requirements on the control gains. The present work also removes the implicit assumption that there is no activation overlap. The developed controller is implemented on six individuals with asynchronous and conventional stimulation. Asynchronous stimulation is found to result in statistically longer durations of successful tracking for the knee-joint angle despite statistically different responses between the stimulation channels.

II. Limb Model

The knee-joint dynamics are modeled as in [30] as

$$M_I + M_e + M_g + M_v + \tau_d = \tau \tag{1}$$

where $M_I : \mathbb{R} \to \mathbb{R}$ denotes the effect of inertia of the lower leg about the knee-joint; $M_e : \mathbb{R} \to \mathbb{R}$ denotes elasticity due to joint stiffness; $M_g : \mathbb{R} \to \mathbb{R}$ denotes the effect of gravity; $M_v : \mathbb{R} \to \mathbb{R}$ denotes the viscous effects due to damping in the musculotendon complex; $\tau_d \in \mathbb{R}$ denotes a bounded, unknown, time-varying disturbance from unmodeled dynamics such that $|\tau_d| \le \overline{\tau}_d$ where $\overline{\tau}_d \in \mathbb{R}$ is a known positive bound; and $\tau \in \mathbb{R}$ denotes the knee-joint torque that is produced due to stimulation. The effects of inertia and gravity in (1) are modeled as

$$M_I \triangleq J\ddot{q}, \quad M_g \triangleq mgl\sin(q) \tag{2}$$

where $J, m, g, l \in \mathbb{R}$ are positive constants, and $q, \dot{q}, \ddot{q} \in \mathbb{R}$ denote the angular position (depicted in Fig. 1), velocity, and acceleration of the shank about the knee-joint, respectively. The terms J, m, and l denote the unknown inertia of the combined shank and foot, the unknown mass of the lower leg, and the unknown distance between the knee-joint and the lumped center of mass of the lower leg, respectively, while g denotes the gravitational acceleration. The elastic and viscous effects are modeled as

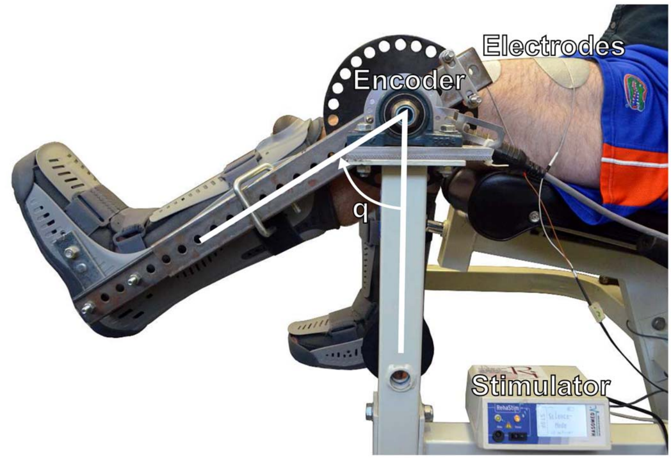

Fig. 1. Modified leg extension machine was fitted with optical encoders to measure the knee-joint angle and provide feedback to the developed control algorithm running on a personal computer. The desired stimulation parameters were then sent to the stimulator via USB.

$$M_e \triangleq k_{e_1}\big(\exp\big(-k_{e_2}q\big)\big)\big(q - k_{e_3}\big)$$

where $k_{e_1}, k_{e_2}, k_{e_3} \in \mathbb{R}$ are unknown constants and

$$M_v \triangleq -B_1 \tanh(-B_2\dot{q}) + B_3\dot{q}$$

where $B_1, B_2, B_3 \in \mathbb{R}$ are unknown positive constants.

During asynchronous stimulation, there are $N \in \mathbb{N}$ stimulation channels in the system. Since each stimulation channel is expected to activate differing sets of motor units, the resulting dynamics depend on the active stimulation channel. Let $\mathbb{S} \subset \mathbb{N}$ be the finite index set for all involved subsystems (i.e., the stimulation channels) defined as $\mathbb{S} = \{1, 2, 3, \ldots, N\}$. The torque produced by stimulation of the ith subsystem is related to the musculotendon force as

$$\tau_i \triangleq \varsigma_i F_{T,i}, \ i \in \mathbb{S} \tag{3}$$

where $\varsigma_i \in \mathbb{R}$ denotes a positive moment arm that changes with extension and flexion of the leg. The musculotendon force $F_{T,i} \in \mathbb{R}$ in (3) is defined as

$$F_{T,i} \triangleq F_i \cos(a_i), \ i \in \mathbb{S} \tag{4}$$

where $a_i \in \mathbb{R}$ is the pennation angle between the tendon and the muscle which changes with extension and flexion of the leg, and $F_i \in \mathbb{R}$ is the force produced by the recruited muscle fibers in the ith subsystem. The relationship between muscle force and applied voltage is denoted by the unknown function $\eta_i \in \mathbb{R}$ as

$$F_i \triangleq \eta_i V_i, \ i \in \mathbb{S} \tag{5}$$

where $V_i \in \mathbb{R}$ represents the voltage applied to the ith subsystem by electrical stimulation. To facilitate the subsequent

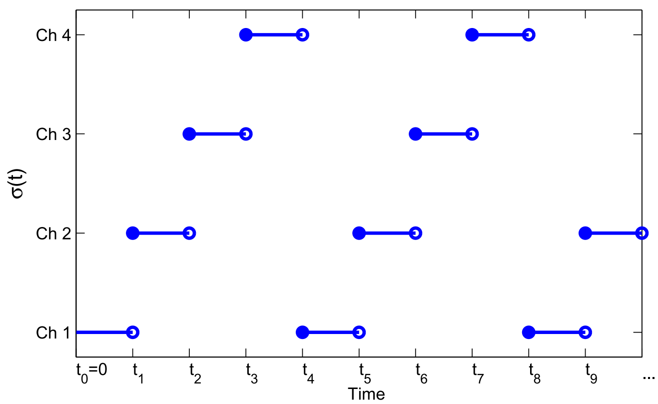

Fig. 2. Example switching signal for four-channel asynchronous stimulation. The vertical axis denotes the stimulation channel selected by the switching signal as a function of time. While the particular choice of σ in the present example corresponds to the manner of switching employed in previous asynchronous stimulation literature, the mathematical framework of the present work does not require switching to happen in any particular order.

analysis, let $\Omega_i \in \mathbb{R}$ be a positive auxiliary term, defined as in [30] as

$$\Omega_i \triangleq \varsigma_i \eta_i \cos(a_i),\ i \in \mathbb{S}. \tag{6}$$

From (3)–(6), the torque produced by stimulation of the ith subsystem is then related to the voltage applied to the ith subsystem as

$$\tau_i = \Omega_i V_i,\ i \in \mathbb{S}. \tag{7}$$

Assumption 1: The moment arm ς_i is assumed to be a continuous, nonzero, positive, bounded function [39]. The function η_i is assumed to be a continuous, nonzero, positive, and bounded function [40]. Thus from (6), Ω_i is assumed to be a continuous, nonzero, positive, and bounded function such that $\Omega_i > \underline{\Omega} > 0,\ \forall i \in \mathbb{S}$ where $\underline{\Omega} \in \mathbb{R}$ is a known positive constant.

During asynchronous stimulation, the active stimulation channel is switched according to a predefined sequence (selected by the user) where only one channel is activated at a given time. To describe this phenomenon, let $\sigma : [t_0, \infty) \to \mathbb{S}$ denote a piecewise constant signal which selects a subsystem from $\mathbb{S}$ to be activated at time t, where $t_0 \in \mathbb{R}$ is the initial time. The voltage delivered to each subsystem, V_i, is then described in terms of the switching signal as

$$V_i(t) = \begin{cases} v_i(t) & \sigma(t) = i,\ i \in \mathbb{S} \\ 0 & \text{otherwise} \end{cases} \tag{8}$$

where $v_i \in \mathbb{R}$ denotes the subsequently designed control voltage for the ith subsystem.

Property 1: The designed switching signal σ has a finite number of switching instances on any bounded time interval and the switching signal σ remains constant for $t \in [t_k, t_{k+1})$, $k \in \mathbb{N}$, where t_k denotes the instances of time when the active stimulation channel is switched. An example switching signal is illustrated in Fig. 2 for four-channel stimulation.

After utilizing (7) and (8), the knee-joint dynamics in (1) can be expressed as

$$M_I + M_e + M_g + M_v + \tau_d = \Omega_{\sigma(t)} v_{\sigma(t)} \tag{9}$$

where the inertial, gravitational, elastic, and viscous components are common to all subsystems since all subsystems act on the same knee-joint. In (9), while each of the terms vary with time in general, the time dependence of $\Omega_{\sigma(t)}$ is explicitly written to highlight that the control effectiveness instantly switches its value due to the switching signal σ, which characterizes the switching nature of asynchronous stimulation.

III. Control Development

The goal is to develop a controller that enables the knee-joint to track a desired angular trajectory. To facilitate the subsequent development, let $e_0 \in \mathbb{R}$ be defined as

$$e_0 \triangleq \int_{t_0}^{t} (q_d(s) - q(s))ds \tag{10}$$

where $q_d \in \mathbb{R}$ is a desired angular trajectory for the knee-joint, which is designed such that $q_d, \dot{q}_d, \ddot{q}_d \in \mathcal{L}_\infty$. To facilitate the subsequent development, the auxiliary tracking errors $e_1, e_2 \in \mathbb{R}$ are defined as

$$e_1 \triangleq \dot{e}_0 + \alpha_0 e_0 \tag{11}$$

$$e_2 \triangleq \dot{e}_1 + \alpha_1 e_1 \tag{12}$$

where $\alpha_0, \alpha_1 \in \mathbb{R}$ denote selectable positive constants.

Remark 1: Part of the motivation for designing e_1 and e_2 as in (11) and (12) is to include an integrator in the subsequently developed controller. It will later be shown that $|e_0|, |e_1| \to 0$, which implies $|q_d - q| \to 0$, thereby achieving the control objective.

After multiplying the time derivative of (12) by J, and utilizing (2) and (9)–(11), the open-loop dynamics during asynchronous stimulation can be expressed as

$$J\dot{e}_2 = W + \tau_d - \Omega_{\sigma(t)} v_{\sigma(t)} \tag{13}$$

where J is the same inertia for each subsystem since each subsystem acts on the same knee-shank complex, and $W \in \mathbb{R}$ denotes an auxiliary term defined as

$$W \triangleq J(\ddot{q}_d + \alpha_0(\dot{q}_d - \dot{q}) + \alpha_1 \dot{e}_1) + M_e + M_g + M_v.$$

To facilitate the subsequent stability analysis, (13) is expressed as

$$J\dot{e}_2 = \tilde{W} + W_d - e_1 + \tau_d - \Omega_{\sigma(t)} v_{\sigma(t)} \tag{14}$$

where $\tilde{W}, W_d \in \mathbb{R}$ denote the auxiliary terms

$$\tilde{W} \triangleq W - W_d + e_1$$
$$W_d \triangleq J\ddot{q}_d + M_e(q_d) + M_g(q_d) + M_v(\dot{q}_d).$$

The motivation for expressing the open-loop error system as in (14) is to separate the model into groups that are bounded by states or by constants. Specifically, by applying the mean value theorem [41, Lemma 5], $\tilde{W}$ can be upper bounded by state-dependent terms as

$$\left|\tilde{W}\right| \leq \rho(\|z\|)\|z\| \tag{15}$$

where $\|\cdot\|$ denotes the standard 2-norm, $z \in \mathbb{R}^3$ is defined as

$$z \triangleq [e_0,\ e_1,\ e_2]^T \tag{16}$$

and $\rho : \mathbb{R} \to \mathbb{R}$ is a positive, radially unbounded, and nondecreasing function. Based on the assumption that the desired angular trajectory of the knee-joint is bounded, an upper bound for W_d can be developed as

$$|W_d| \leq \overline{W}_d \tag{17}$$

where $\overline{W}_d \in \mathbb{R}$ is a known positive constant.

Based on the open-loop error system in (14) and the subsequent stability analysis, a sliding-mode-based controller is designed as

$$v_i \triangleq \left(k_{1,i} + k_{2,i}\right)e_2 + k_{3,i}\,\mathrm{sgn}(e_2),\ i \in \mathbb{S} \tag{18}$$

where $k_{1,i},\ k_{2,i},\ k_{3,i} \in \mathbb{R}$ are positive, constant control gains, and $\mathrm{sgn}(\cdot)$ denotes the signum function. To facilitate the subsequent analysis, let the minimum control gains for all stimulation channels be defined as

$$k_{1,\min} \triangleq \min_{i\in\mathbb{S}}\left\{k_{1,i}\right\} \tag{19}$$

$$k_{2,\min} \triangleq \min_{i\in\mathbb{S}}\left\{k_{2,i}\right\} \tag{20}$$

$$k_{3,\min} \triangleq \min_{i\in\mathbb{S}}\left\{k_{3,i}\right\}. \tag{21}$$

After substituting (18) into (14), the closed-loop dynamics can be written as

$$J\dot{e}_2 = \tilde{W} + W_d - e_1 + \tau_d - \Omega_{\sigma(t)}\left(k_{1,\sigma(t)} + k_{2,\sigma(t)}\right)e_2 - \Omega_{\sigma(t)}k_{3,\sigma(t)}\,\mathrm{sgn}(e_2).$$

As described in the Appendix, Theorem 1 and its associated stability proof establish that the switching asynchronous controller in (8) and (18) yields exponential tracking of a desired knee-joint trajectory.

IV. Experiments

Asynchronous and conventional stimulation were tested during isometric contractions to examine the muscle response to stimulation (i.e., the control effectiveness). Experiments were also conducted with dynamic contractions to test the developed controller and to better understand the NMES-induced fatigue characteristics of asynchronous and conventional stimulation during feedback control. For dynamic contractions, the developed control algorithm was used to vary the pulsewidth in real time while the current amplitude and stimulation frequency remained constant. Meanwhile, for the isometric experiments, the pulsewidth was varied open-loop (i.e., predetermined).

A. Subjects

Six able-bodied individuals (male, aged 20 to 27) participated in the study. Prior to participation, written informed consent was obtained from all participants, as approved by the institutional review board at the University of Florida.

B. Apparatus

A commercial leg extension machine (shown previously in Fig. 1) was modified for the present experiments. Orthotic boots were added to the machine to securely fasten the shank and foot. The modified leg extension machine allowed adjustments to ensure the axis of rotation of the knee-joint aligned with that of the machine. Optical encoders (BEI Technologies) were installed along the axis of rotation for the purpose of measuring the knee-joint angle for feedback control during the dynamic experiments. The encoders yield 20 000 ticks per revolution after utilizing quadrature, resulting in a resolution of 0.018 degrees. The encoder signal was recorded by a data acquisition device (Quanser Q8-USB) to provide angular position and velocity measurements to the developed controller during the dynamic experiments. The control algorithm was implemented on a personal computer running a compiled Simulink program at 1000 Hz. A current-controlled 8-channel stimulator (RehaStim, Hasomed GmbH, operating in ScienceMode) received the desired stimulation parameters via USB and delivered the stimulation to surface electrodes (Axelgaard Manufacturing Co., Ltd.)[1] placed over the quadriceps femoris muscle group. These stimulation parameters were calculated by the controller in the case of the dynamic experiments and were predetermined in the case of the isometric experiments. During isometric experiments, the knee-joint was fixed to a constant angle by connecting force transducers (Transducer Techniques) between the base of the leg extension machine and the metal linkage attached to the boots. The analog voltage provided by the force transducers was amplified and then recorded by the data acquisition device. This signal was then converted to knee-joint torque based on previously performed calibration.

C. Stimulation Protocols

Two stimulation protocols were examined: 1) 16 Hz asynchronous stimulation (A16) with four channels and 2) 64 Hz conventional stimulation (C64) with a single channel. These two protocols were selected because A16 has a composite stimulation frequency equivalent to C64. Conventional stimulation consisted of a single stimulation channel with a pair of 3” by 5” Valutrode surface electrodes placed distally and proximally over the quadriceps femoris muscle group, while asynchronous stimulation consisted of four channels of stimulation utilizing four electrodes placed distally (1.5” by 3.5” Valutrode) and two electrodes placed proximally (2” by 3.5” Valutrode). The electrode configurations utilized for conventional and asynchronous stimulation are depicted in Fig. 3.

D. Precautions

The order of the two stimulation protocols (A16 and C64) were randomized for each leg. To prevent any layover effect of fatigue, each leg received only one stimulation protocol per day. A minimum of 48 h of rest was required before the

[1]Surface electrodes for the study were provided compliments of Axelgaard Manufacturing Co., Ltd.

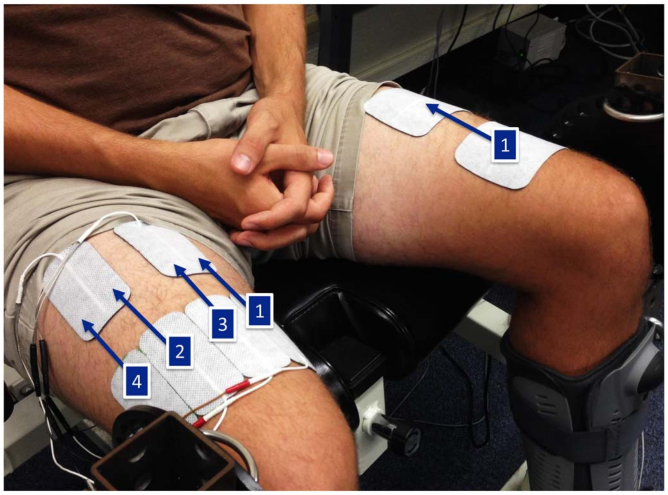

Fig. 3. Depicted are the two electrode configurations utilized in the study. Conventional stimulation (individual's left leg) consists of one stimulation channel with a pair of surface electrodes placed proximally and distally. Four-channel asynchronous stimulation (individual's right leg) utilizes four stimulation channels with two surface electrodes placed proximally, and four placed distally. As depicted, asynchronous stimulation channels 1 and 3 share the most medial and proximal electrode, while channels 2 and 4 share the most lateral and proximal electrode.

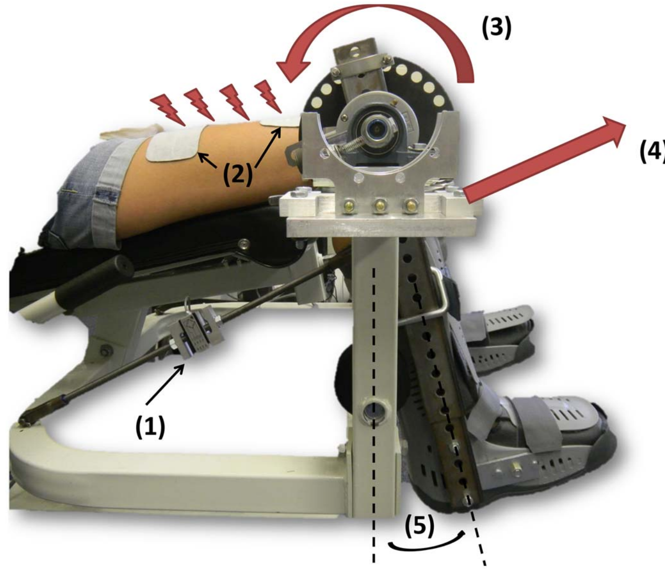

Fig. 4. Isometric testbed. To measure the control effectiveness, force transducers (1) were attached between the base of the machine and the metal linkage (attached to the boots) to secure the leg. The shank was fixed at a constant angle (5) of approximately 15 degrees with respect to vertical. Given the inclination of the thigh with respect to the ground plane, the resulting knee-joint angle was approximately 90 degrees, as depicted. Stimulation was applied via surface electrodes (2) and the measured force (4) from the force transducers was converted to isometric knee-joint torque (3) for subsequent analysis.

individual completed the remaining stimulation protocol for each leg.

E. Measuring the Control Effectiveness

Due to the spatial distribution of the electrodes, it is expected that the muscle response to stimulation will be different for each channel when utilizing asynchronous stimulation. To examine the extent of the differences, recruitment curves (i.e., the relationship between pulsewidth and the evoked torque) were constructed for each channel with the knee-joint fixed at a constant angle, as depicted in Fig. 4. To construct the recruitment curves, pulses were delivered at 64 Hz with a constant current amplitude of 70 mA and a pulsewidth that increased as a ramp (increasing in steps of 1 μs until the torque reached 25 N·m or the participant reported mild discomfort). The control effectiveness for each channel was then calculated as the linear slope of the recruitment curve. The control effectiveness was also calculated for conventional stimulation as a point of reference.

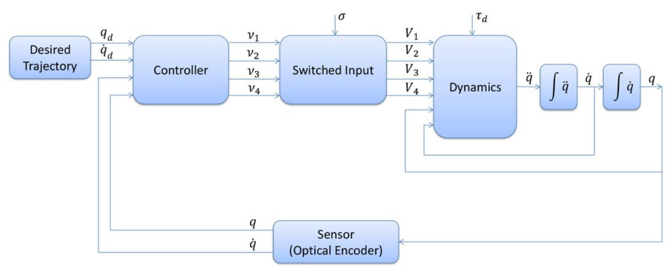

Fig. 5. Block diagram. The objective of the fatigue trials was to examine how long each stimulation protocol could yield limb tracking within a predefined acceptable tolerance (i.e., the SRT). The measured and desired joint angles and velocities were utilized by the controller to calculate the stimulation input for each channel (18). The individual channels were then switched on and off according to (8) using the switching signal σ previously depicted in Fig. 2. The desired stimulation parameters were delivered to the stimulator via USB. An optical encoder was affixed to the axis of rotation of the knee-joint. A data acquisition device provided joint angle and velocity measurements based on the encoder signal. These measurements were then returned to the controller, thus closing the feedback loop.

F. Fatigue Trials

After measuring the control effectiveness under isometric conditions, the force transducers were disconnected to allow the limb to move freely, as depicted previously in Fig. 1. Fatigue trials were then conducted to compare each stimulation protocol in terms of its ability to maintain limb trajectory tracking. The desired angular trajectory[2] of the knee-joint was selected as a sinusoid ranging from 5 to 50 degrees with a period of 2 s. The current amplitude and stimulation frequency remained constant while the pulsewidth was adjusted according to the developed feedback control algorithm in (18) and the stimulation channels were switched according to (8) and Fig. 2. A block diagram of the control scheme is provided in Fig. 5. Since there is a finite pulsewidth resolution for the stimulator (steps of 1 μs), the current amplitude must be selected small enough so that there is a sufficient range of pulsewidth values corresponding to the desired range of motion. However, the current amplitude must also be selected large enough so that the pulsewidth does not saturate. Based on preliminary experiments, the current amplitude was fixed to 70 mA. However, in the specific case of conventional stimulation with subject B, the current amplitude was increased to 90 mA since the muscle exhibited a weaker response to stimulation. This is

[2]The desired trajectory was based on the comfortable range of motion.

TABLE I
CONTROL EFFECTIVENESS ($N{\cdot}m{\cdot}\mu s^{-1}$)

	Conv	Async*			
Subject-Leg	**Ch 1**	**Ch 1**	**Ch 2**	**Ch 3**	**Ch 4**
A - Left	0.483	0.743	0.566	0.403	0.289
A - Right	0.404	0.404	0.217	0.333	0.258
B - Left	0.112	0.214	0.070	0.135	0.267
B - Right	0.146	0.193	0.044	0.144	0.089
C - Left	0.396	0.367	0.115	0.318	0.322
C - Right	0.203	0.374	0.197	0.286	0.349
D - Left	0.256	0.779	0.182	0.351	0.208
D - Right	0.219	0.337	0.138	0.121	0.271
E - Left	0.337	0.518	0.179	0.356	0.360
E - Right	0.229	0.609	0.365	0.512	0.397
F - Left	0.155	0.114	0.049	0.057	0.091
F - Right	0.132	0.179	0.070	0.184	0.070
25th Percentile	**0.148**	**0.198**	**0.070**	**0.137**	**0.120**
Median	**0.224**	**0.372**	**0.159**	**0.300**	**0.269**
75th Percentile	**0.382**	**0.586**	**0.212**	**0.355**	**0.335**

∗ A Friedman test indicated that there was a statistically significant difference between the stimulation channels for the asynchronous electrode configuration in terms of median control effectiveness

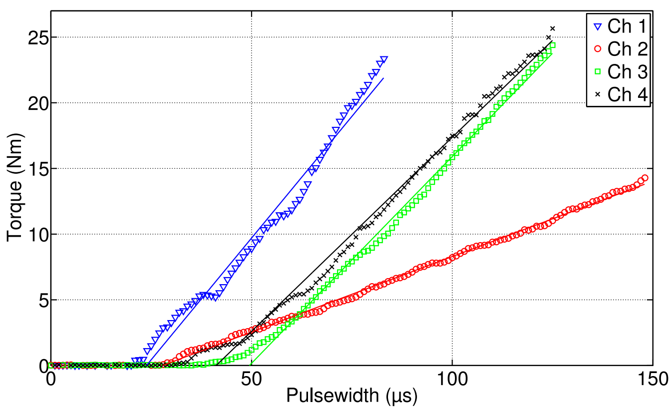

Fig. 6. Recruitment curves corresponding to the four individual channels of asynchronous stimulation on the left leg of subject C. Solid lines indicate the linear fit which illustrates the differences in the control effectiveness for each channel [i.e., Ω in (7)].

unsurprising since conventional stimulation has been reported to require a larger current amplitude to reach the same value of torque as asynchronous stimulation [11], [23], [25].

Control gains were adjusted in pretrial tests to achieve trajectory tracking. The root mean square (RMS) position tracking error was calculated in real time with a moving window of 2 s to assist the gain tuning process (targeting five degrees of RMS error). The baseline RMS tracking error was calculated when the tracking error had reached steady state.[3] The successful run time (SRT) of each fatigue trial was then calculated as the elapsed time from the onset of steady state tracking to the time that the RMS tracking error increased to three degrees above the baseline measurement.

[3]The onset of steady state tracking is defined as the point at which the RMS error begins to flatten (no longer decreasing from the large initial error). Steady state tracking occurred approximately 10 s after starting the trial, on average.

TABLE II
SRT (IN SECONDS)

Subject-Leg	**C64**	**A16**	**Difference**
A - Left	24.5	44.3	19.7
A - Right	28.5	58.0	29.5
B - Left	25.9	56.8	30.9
B - Right	29.7	68.4	38.7
C - Left	36.7	59.6	23.0
C - Right	48.9	80.1	31.2
D - Left	27.3	234.8	207.5
D - Right	20.7	95.3	74.5
E - Left	23.5	38.2	14.7
E - Right	31.3	55.2	23.9
F - Left	26.9	35.8	8.8
F - Right	33.2	60.3	27.1
25th Percentile	**24.9**	**47.0**	**20.5**
Median	**27.9**	**58.8**	**28.3***
75th Percentile	**32.8**	**77.2**	**36.8**

∗ SRT of asynchronous stimulation is statistically longer than that of conventional stimulation (58.8 seconds versus 27.9 seconds)

TABLE III
BASELINE RMS ERROR (DEGREES)

Subject-Leg	**C64**	**A16**	**Difference**
A - Left	5.46	5.50	0.04
A - Right	5.29	5.32	0.02
B - Left	5.05	5.18	0.13
B - Right	5.02	5.23	0.21
C - Left	4.90	4.72	-0.18
C - Right	5.03	4.63	-0.40
D - Left	5.05	5.38	0.33
D - Right	5.36	5.10	-0.26
E - Left	5.77	5.76	-0.01
E - Right	5.41	4.54	-0.87
F - Left	5.40	5.28	-0.12
F - Right	5.43	5.53	0.10
25th Percentile	**5.03**	**4.81**	**-0.24**
Median	**5.33**	**5.26**	**0.01**
75th Percentile	**5.42**	**5.47**	**0.12**

No significant differences were determined between the two protocols in terms of baseline RMS error (5.33 degrees versus 5.26 degrees)

G. Statistical Analysis

A Wilcoxon signed rank test was performed at a significance level of $\alpha = 0.05$ to test for statistically significant differences between asynchronous and conventional stimulation in terms of SRT, the onset of steady state tracking, and the baseline RMS tracking error. A Friedman test was performed at a significance level of $\alpha = 0.05$ to test for statistically significant differences between the four asynchronous stimulation channels in terms of the control effectiveness.

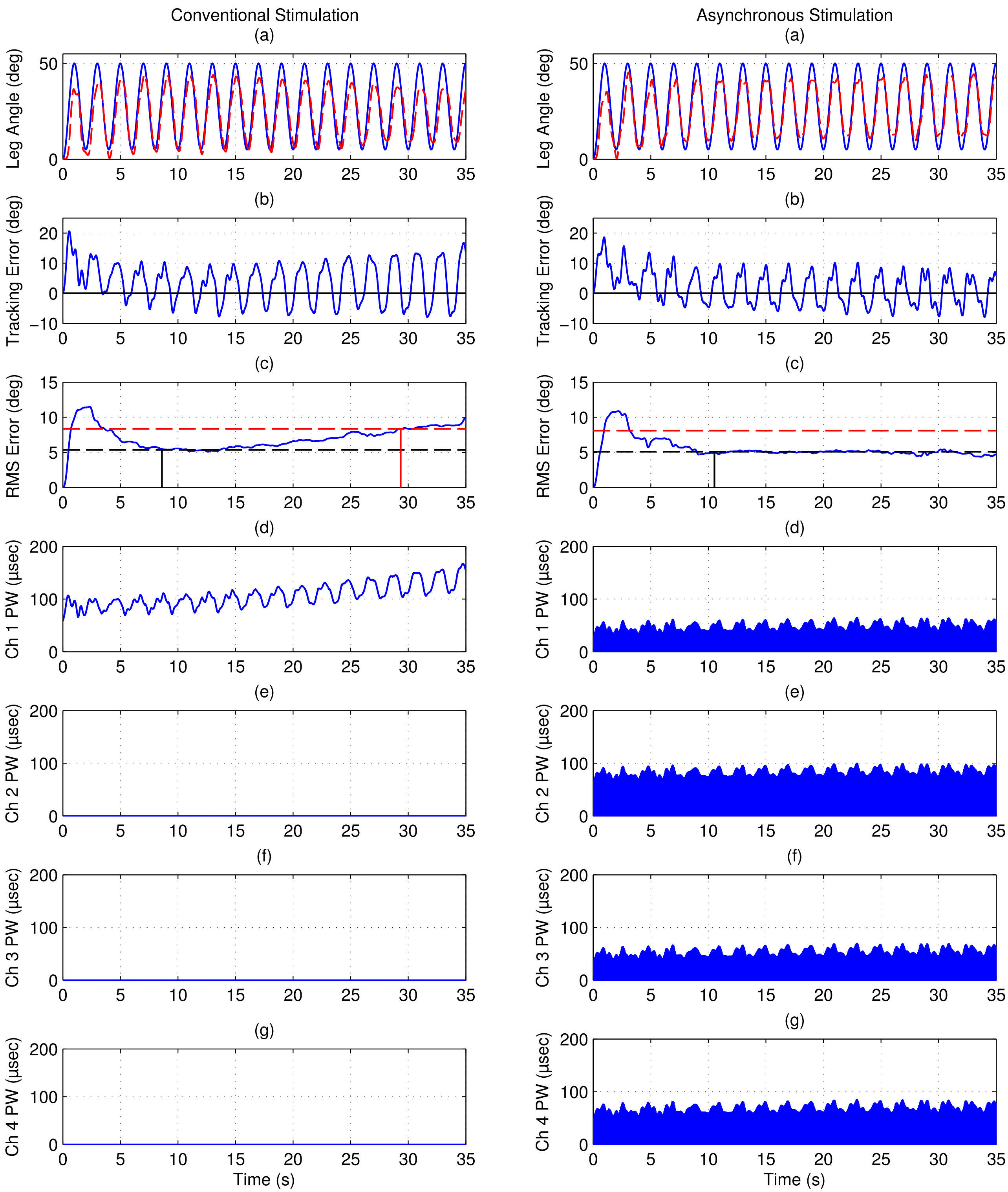

Fig. 7. Example tracking performance taken from the right leg of subject D comparing conventional stimulation (left column) and asynchronous stimulation (right column). Plot (a) depicts the desired (solid line) and actual (dashed line) knee-joint angle. Plot (b) depicts the angular position tracking error. Plot (c) depicts the RMS tracking error calculated over a moving 2 s window (corresponding to the period of the desired trajectory). The horizontal dashed lines in plot (c) indicate the baseline error and the threshold that determines the end of successful tracking (set to 3 degrees of RMS error above the baseline measurement). Vertical solid lines correspond to the time that steady state tracking began and the time that the RMS error increased by 3 degrees. The end time is not shown for asynchronous stimulation so that the two protocols can be visually compared over the same time scale. Plots (d)–(g) depict the pulsewidth inputs calculated by the controller. The shaded appearance of plots (d)–(g) for asynchronous stimulation is due to the switching nature of asynchronous stimulation and the time scale of the plot. A more detailed view of the switched control input is provided in Fig. 8.

V. Results

Table I lists the control effectiveness for single-channel conventional stimulation as well as the control effectiveness for each channel of asynchronous stimulation. A Friedman test on the control effectiveness of the four asynchronous stimulation channels indicated that there was a statistically

TABLE IV
ONSET OF STEADY STATE TRACKING (IN SECONDS)

Subject-Leg	C64	A16	Difference
A - Left	5.5	8.8	3.3
A - Right	8.9	10.8	1.9
B - Left	6.9	11.2	4.3
B - Right	5.2	8.6	3.4
C - Left	11.3	20.2	9.0
C - Right	13.5	5.7	-7.8
D - Left	15.1	8.6	-6.5
D - Right	8.6	11.3	2.7
E - Left	11.4	6.9	-4.6
E - Right	11.6	9.0	-2.6
F - Left	10.7	13.0	2.4
F - Right	9.9	13.8	3.9
25th Percentile	**7.4**	**8.6**	**-4.1**
Median	**10.3**	**9.9**	**2.5**
75th Percentile	**11.5**	**12.6**	**3.8**

No significant differences were determined between the two protocols in terms of the onset of steady state tracking (10.3 versus 9.9 seconds)

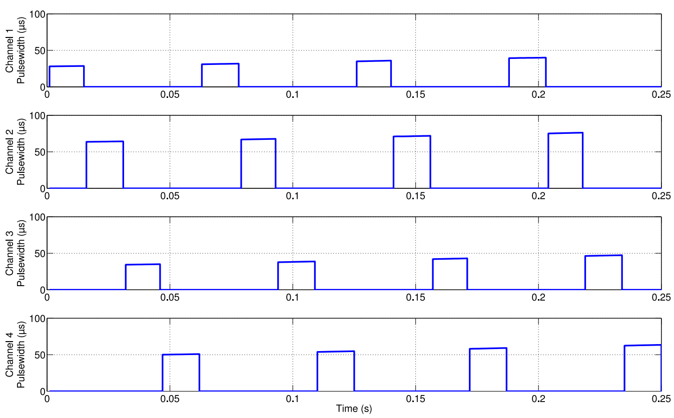

Fig. 8. For asynchronous stimulation, the control inputs for each channel were calculated according to (18) and the stimulation channels were switched according to (8). Depicted are the control inputs for the asynchronous stimulation fatigue trial of the right leg of subject D. For illustrative purposes, the control inputs are depicted over a period of 0.25 s.

significant difference between the channels (p-value $= 0.000$), with the channels 1 and 2 differing by more than a factor of two (median across all subjects). Fig. 6 depicts the measured recruitment curves for the left leg of subject C, highlighting each channel's differing response to electrical stimulation. The SRTs for each fatigue trial are listed in Table II, with the corresponding baseline RMS error and onset of steady state tracking listed in Tables III and IV, respectively. Asynchronous stimulation yielded a significantly longer SRT than conventional stimulation (p-value $= 0.003$), approximately doubling the SRT (58.8 s versus 27.9 s). Meanwhile, the baseline RMS error was not significantly different (p-value $= 0.666$), with median values of 5.33 and 5.26 degrees for conventional and asynchronous stimulation, respectively. Similarly, the onset of steady state tracking was not significantly different (p-value $= 0.666$), with median values of 10.3 and 9.9 s for conventional and asynchronous stimulation, respectively. Example fatigue trials comparing asynchronous and conventional stimulation are shown in Fig. 7. A detailed view highlighting the switched control input for each stimulation channel is provided in Fig. 8.

VI. CONCLUSION

Asynchronous stimulation is a promising stimulation method that has been previously shown to reduce fatigue during isometric contractions with fixed stimulation parameters [15], [16], [19]–[26], [28]. Asynchronous stimulation may also reduce fatigue during isotonic gripping [18] and FES cycling [13]. The desire to use asynchronous stimulation for rehabilitative procedures or neuroprostheses, coupled with the challenges of switching between sets of motor units, motivates the developed control design. A challenge to designing an asynchronous stimulation controller is that, due to the spatial distribution of the electrodes, each channel is likely to recruit a different number or type of motor units for the same stimulation parameters. From a control perspective, this problem is represented by a switching control effectiveness [$\Omega_{\sigma(t)}$ in (9)]. While previous studies have not directly measured the control effectiveness for each channel, there is some previous evidence to suggest that each channel's response to stimulation can differ since asynchronous stimulation has been shown to result in force ripple (i.e., unfused tetanus) [11], [19]. In the present study, the control effectiveness was measured for each channel during isometric contractions. The results indicate that there is in fact a significant difference, corroborating the switched model in (9). It should be noted that the control effectiveness for each channel is time-varying in general (e.g., due to fatigue and the muscle force-length relationship), and therefore, the control effectiveness for each channel may become more similar or dissimilar as the leg moves and the muscle fatigues during feedback control. Nevertheless, the present results highlight that the control effectiveness values should not be assumed to be equal when developing control algorithms for asynchronous stimulation.

Limited control development has been provided for multichannel asynchronous stimulation. Lau *et al.* [27] implemented a closed-loop, logic-based, if-then-else algorithm for standing in cats. Frankel *et al.* [36] implemented an iterative learning controller for isometric force control in cats. However, no modeling or stability analysis were included in the aforementioned studies. In [37], an RISE-based control law was developed for knee-joint tracking with asynchronous stimulation. While the work considered that each stimulation channel could have a different control effectiveness, the control design did not allow for instantaneous switching and made an implicit assumption that there is no activation overlap between the stimulation channels. Therefore, in the present work, a switched systems analysis was used to examine and develop an alternative control approach that allows for instantaneous switching between stimulation channels and removes the assumption that there is no activation overlap. The developed controller was implemented on six individuals with asynchronous and conventional stimulation. Asynchronous stimulation was found to result in statistically longer durations of successful tracking for the knee-joint angle despite statistically different responses between the stimulation channels. Although there were individual differences which could be due to differences in muscle physiology or conditioning, asynchronous stimulation outperformed conventional stimulation in terms of SRT in every trial (Table II). This result is promising as longer SRTs indicate that asynchronous stimulation could lead to longer treatment durations for closed-loop rehabilitation. Similarly, longer SRTs indicate that asynchronous stimulation could potentially be utilized in assistive devices to extend the duration that a functional task can be achieved.

While the present results are promising, additional opportunities exist for asynchronous stimulation. For example, when asked to qualitatively compare the two protocols, participants reported the sensation of asynchronous stimulation to be more unpleasant than conventional stimulation. This may simply be due to the fact that asynchronous stimulation had longer SRTs. However, it may also be due to increased current densities via smaller electrode coverage. It is possible that selection of an optimal electrode configuration or perhaps modulating the stimulation intensity for each channel based on its relative sensitivity to stimulation may alleviate this issue. Along these lines, an adaptive control design may prove to be beneficial for asynchronous stimulation. Specifically, adaptive controllers typically require less control effort and result in better tracking performance than robust controllers in practice, and reduced stimulation intensities could lead to increased comfort. Future efforts could also focus on extending the current result to other functional activities. For example, asynchronous stimulation has shown the potential to be effective for open-loop FES cycling with constant stimulation parameters [13], but combining feedback control of FES cycling [42] with asynchronous stimulation may further improve rehabilitative treatments. Along these lines, opportunities exist whereby asynchronous stimulation could be implemented along with an exoskeleton (see [43]–[45]) or robotic orthosis (see [46]) to create a stimulation-assisted exoskeleton/orthosis that exploits the fatigue-resistant characteristics of asynchronous stimulation.

In conclusion, feedback control of asynchronous stimulation should also be examined in a patient population. While the present results are promising, significant additional testing beyond the scope of this paper is needed to determine clinical efficacy. Specifically, different disease and injury populations will potentially respond differently to electrical stimulation and may exhibit muscle atrophy. Therefore, the duration of successful tracking may differ from that of the able-bodied population in the present study. Nevertheless, asynchronous stimulation is still expected to be advantageous over conventional stimulation in terms of extending the SRT, as highlighted in the present study. Extended SRTs indicate the potential for prolonged treatment durations or increasing the number of successful repetitions of a functional task. However, disease-specific clinical trials are needed to shed light on clinical impact.

Appendix

Let $\mathcal{D}$ be the interior of the set $\{\xi \in \mathbb{R}^3 | \rho(\|\xi\|) < \sqrt{4\lambda k_{2,\min}\underline{\Omega}}\}$ where

$$\lambda \triangleq \min\left\{\left(\alpha_0 - \frac{1}{2}\right),\ \left(\alpha_1 - \frac{1}{2}\right),\ k_{1,\min}\underline{\Omega}\right\} \tag{22}$$

and $\underline{\Omega}$ was defined in Assumption 1. Let $V_L : \mathcal{D} \to \mathbb{R}$ be a common Lyapunov function candidate, defined as

$$V_L \triangleq \frac{1}{2}e_0^2 + \frac{1}{2}e_1^2 + \frac{1}{2}Je_2^2 \tag{23}$$

which satisfies the following inequalities:

$$\lambda_1\|z\|^2 \le V_L \le \lambda_2\|z\|^2 \tag{24}$$

where $\lambda_1 \triangleq \min\{(1/2), (1/2)J\}$, $\lambda_2 \triangleq \max\{(1/2), (1/2)J\}$, and z was defined in (16). Let the region of attraction $\mathcal{D}_z \subset \mathcal{D}$ be the interior of $\{\xi \in \mathcal{D} | \rho(\sqrt{(\lambda_2/\lambda_1)}\|\xi\|) < \sqrt{4\lambda k_{2,\min}\underline{\Omega}}\}$.

Theorem 1: The controller designed in (8) and (18) yields semi-global exponential tracking in the sense that

$$|q_d(t) - q(t)| \le (1+\alpha_0)\sqrt{\frac{\lambda_2}{\lambda_1}}\|z(t_0)\|e^{-\frac{c}{2\lambda_2}(t-t_0)} \tag{25}$$

where t_0 is the initial time, and $c \in \mathbb{R}$ is some positive constant, provided that the control gain $k_{2,\min}$ is selected sufficiently large so that the initial condition $z(t_0) \in \mathcal{D}_z$; $\alpha_0, \alpha_1 > (1/2)$; and the control gain $k_{3,\min}$ is selected according to the following sufficient condition:

$$k_{3,\min} > \underline{\Omega}^{-1}\left(\overline{W}_d + \overline{\tau}_d\right) \tag{26}$$

where $\overline{W}_d$ was introduced in (17), and $\overline{\tau}_d$ is a known bound on the disturbance torque.

Proof: The time derivative of (23) exists almost everywhere (a.e.), i.e., for almost all $t \in [t_0, \infty)$, and $\dot{V}_L \overset{a.e.}{\in} \dot{\tilde{V}}_L$ where

$$\dot{\tilde{V}}_L \triangleq \bigcap_{\xi \in \partial V_L} \xi^T K[\dot{e}_0,\ \dot{e}_1,\ \dot{e}_2,\ 1]^T \tag{27}$$

where ∂V_L is the generalized gradient of V_L, and $K[\cdot]$ is defined as in [47]. Since V_L is continuously differentiable with respect to its arguments, (27) can be rewritten as

$$\dot{\tilde{V}}_L \subset \nabla V_L^T K[\dot{e}_0,\ \dot{e}_1,\ \dot{e}_2,\ 1]^T \tag{28}$$

where $\nabla V_L \triangleq [e_0,\ e_1,\ e_2 J,\ (1/2)\dot{J}e_2^2]^T$. Using $K[\cdot]$ from [47], the fact that $\dot{J} = 0$, and substituting (11), (12), and (14) into (28) yields

$$\begin{aligned}\dot{\tilde{V}}_L \subset\ & e_0(e_1 - \alpha_0 e_0) + e_1(e_2 - \alpha_1 e_1)\\ & + e_2\big(\tilde{W} + W_d - e_1 + \tau_d - K\big[\Omega_{\sigma(t)}\nu_{\sigma(t)}\big]\big).\end{aligned}$$

First $\dot{V}_L$ is examined during the nonswitching instants to prove that V_L is a common Lyapunov function. Assuming the arbitrary subsystem $p \in \mathbb{S}$ is active at time t

$$\begin{aligned}\dot{\tilde{V}}_L \subset\ & e_0(e_1 - \alpha_0 e_0) + e_1(e_2 - \alpha_1 e_1)\\ & + e_2\big(\tilde{W} + W_d - e_1 + \tau_d - \Omega_p K\big[\nu_p\big]\big),\ p \in \mathbb{S}\end{aligned} \tag{29}$$

where Ω_p is continuous by Assumption 1 and thus $K[\Omega_p \nu_p] = \Omega_p K[\nu_p]$ during the nonswitching instants for arbitrary $p \in \mathbb{S}$.

By canceling common terms and substituting (18), (29) can be rewritten as

$$\dot{\tilde{V}}_L = -\alpha_0 e_0^2 - \alpha_1 e_1^2 + e_0 e_1 + e_2\big(\tilde{W} + W_d + \tau_d\big) - \Omega_p\big(k_{1,p} + k_{2,p}\big)e_2^2 - \Omega_p k_{3,p}|e_2|,\ p \in \mathbb{S} \quad (30)$$

where the set in (29) reduces to the singleton in (30) since $e_2 K[\,\mathrm{sgn}\,](e_2) = |e_2|$. After using Young's inequality, (17), and the definition of the bounded disturbance, the expression in (30) can then be upper bounded as

$$\dot{V}_L \overset{a.e.}{\le} -\left(\alpha_0 - \frac{1}{2}\right)e_0^2 - \left(\alpha_1 - \frac{1}{2}\right)e_1^2 - k_{1,p}\Omega_p e_2^2 - \big(k_{3,p}\Omega_p - \overline{W}_d - \overline{\tau}_d\big)|e_2| - k_{2,p}\Omega_p {e_2}^2 + e_2\tilde{W}. \quad (31)$$

After utilizing (15), (19)–(21), and (26) and the fact that $\Omega_p > \underline{\Omega} > 0,\ \forall p \in \mathbb{S}$ from Assumption 1, the inequality in (31) can be further upper bounded as

$$\dot{V}_L \overset{a.e.}{\le} -\left(\alpha_0 - \frac{1}{2}\right)e_0^2 - \left(\alpha_1 - \frac{1}{2}\right)e_1^2 - k_{1,\min}\underline{\Omega}e_2^2 - k_{2,\min}\underline{\Omega}e_2^2 + \rho(\|z\|)\|z\||e_2|. \quad (32)$$

After completing the square, (32) can be expressed as

$$\begin{aligned}\dot{V}_L &\overset{a.e.}{\le} -\left(\lambda - \frac{\rho^2(\|z\|)}{4k_{2,\min}\underline{\Omega}}\right)\|z\|^2 \\ &\overset{a.e.}{\le} -c\|z\|^2,\ \forall z \in \mathcal{D} \\ &\overset{a.e.}{\le} -\frac{c}{\lambda_2}V_L,\ \forall z \in \mathcal{D} \end{aligned} \quad (33)$$

where c is a positive constant, ρ was introduced in (15), λ_2 was introduced in (24), and λ was introduced in (22). From the inequality in (33), it can be concluded that V_L is in fact a common Lyapunov function since its time derivative has a common negative definite upper bound for each subsystem. From (33), [48, Corollary 1] can be invoked to show that $z \in D,\ \forall t \ge t_0,\ \forall z(t_0) \in D_z$, and hence, $e_0,\ e_1,\ e_2,\ V_L \in \mathcal{L}_\infty,\ \forall z(t_0) \in \mathcal{D}_z$. From (18) and the fact that $e_2 \in \mathcal{L}_\infty$, the control input for each channel $v_i \in \mathcal{L}_\infty$.

From the inequality in (33) and the fact that $z \in D,\ \forall t \ge t_0$, $\forall z(t_0) \in D_z$

$$V_L(t) \le V_L(t_0)e^{-\frac{c}{\lambda_2}(t-t_0)},\ \forall\, z(t_0) \in \mathcal{D}_z.$$

From (24)

$$\begin{aligned}\|z(t)\| &\le \sqrt{\frac{1}{\lambda_1}V_L(t)} \\ &\le \sqrt{\frac{1}{\lambda_1}V_L(t_0)e^{-\frac{c}{\lambda_2}(t-t_0)}},\quad \forall\, z(t_0) \in \mathcal{D}_z \\ &\le \sqrt{\frac{\lambda_2}{\lambda_1}\|z(t_0)\|^2 e^{-\frac{c}{\lambda_2}(t-t_0)}},\ \forall\, z(t_0) \in \mathcal{D}_z \\ &\le \sqrt{\frac{\lambda_2}{\lambda_1}}\|z(t_0)\|e^{-\frac{c}{2\lambda_2}(t-t_0)},\ \forall\, z(t_0) \in \mathcal{D}_z.\end{aligned}$$

From the definitions of e_1 and z in (11) and (16), $|q_d - q| \le |e_1| + \alpha_0|e_0| \le (1+\alpha_0)\|z\|$, and thus, semi-global exponential tracking of the knee-joint trajectory is achieved in the sense of (25). The region of attraction, $\mathcal{D}_z$, can be expanded arbitrarily by increasing $k_{2,\min}$. Furthermore, the result of stability analysis is independent of the designed switching signal σ. In other words, the switching signal can be arbitrarily designed *a priori* by the user without needing to adhere to dwell time requirements. Limb tracking is therefore achieved for asynchronous stimulation despite instant switching between stimulation channels. ■

ACKNOWLEDGMENT

Any opinions, findings, and conclusions or recommendations expressed in this material are those of the author(s) and do not necessarily reflect the views of the sponsoring agency.

REFERENCES

[1] H. Kern *et al.*, "Home-based functional electrical stimulation rescues permanently denervated muscles in paraplegic patients with complete lower motor neuron lesion," *Neurorehabil. Neural Repair*, vol. 24, no. 8, pp. 709–721, 2010. [Online]. Available: http://nnr.sagepub.com/content/24/8/709.abstract

[2] E. Ambrosini, S. Ferrante, A. Pedrocchi, G. Ferrigno, and F. Molteni, "Cycling induced by electrical stimulation improves motor recovery in postacute hemiparetic patients: A randomized controlled trial," *Stroke*, vol. 42, no. 4, pp. 1068–1073, 2011. [Online]. Available: http://stroke.ahajournals.org/content/42/4/1068.abstract

[3] I. Karabay, A. Dogan, M. D. Arslan, G. Dost, and N. Ozgirgin, "Effects of functional electrical stimulation on trunk control in children with diplegic cerebral palsy," *Disabil. Rehabil.*, vol. 34, no. 11, pp. 965–970, 2012.

[4] M. J. Bellman, T.-H. Cheng, R. J. Downey, and W. E. Dixon, "Stationary cycling induced by switched functional electrical stimulation control," in *Proc. Amer. Control Conf.*, Portland, OR, USA, 2014, pp. 4802–4809.

[5] C.-S. Kim *et al.*, "Stimulation pattern-free control of FES cycling: Simulation study," *IEEE Trans. Syst., Man, Cybern. C, Appl. Rev.*, vol. 38, no. 1, pp. 125–134, Jan. 2008.

[6] R. Cornwall and M. R. Hausman, "Implanted neuroprostheses for restoration of hand function in tetraplegic patients," *J. Amer. Acad. Orthop. Surg.*, vol. 12, no. 2, pp. 72–79, 2004.

[7] S. Ferrante, E. Ambrosini, G. Ferrigno, and A. Pedrocchi, "Biomimetic NMES controller for arm movements supported by a passive exoskeleton," in *Proc. Annu. Int. Conf. IEEE Eng. Med. Biol. Soc. (EMBC)*, San Diego, CA, USA, Sep. 2012, pp. 1888–1891.

[8] R. B. Stein *et al.*, "Long-term therapeutic and orthotic effects of a foot drop stimulator on walking performance in progressive and nonprogressive neurological disorders," *Neurorehabil. Neural Repair*, vol. 24, no. 2, pp. 152–167, 2010.

[9] C. S. Bickel, C. M. Gregory, and J. C. Dean, "Motor unit recruitment during neuromuscular electrical stimulation: A critical appraisal," *Eur. J. Appl. Physiol.*, vol. 111, no. 10, pp. 2399–2407, 2011. [Online]. Available: http://dx.doi.org/10.1007/s00421-011-2128-4

[10] C. M. Gregory and C. S. Bickel, "Recruitment patterns in human skeletal muscle during electrical stimulation," *Phys. Ther.*, vol. 85, no. 4, pp. 358–364, 2005.

[11] R. J. Downey, M. Tate, H. Kawai, and W. E. Dixon, "Comparing the force ripple during asynchronous and conventional stimulation," *Muscle Nerve*, vol. 50, no. 4, pp. 549–555, Oct. 2014.

[12] S. A. Binder-Macleod and W. A. McLaughlin, "Effects of asynchronous stimulation on the human quadriceps femoris muscle," *Arch. Phys. Med. Rehabil.*, vol. 78, no. 3, pp. 294–297, 1997. [Online]. Available: http://www.sciencedirect.com/science/article/pii/S000399939790037X

[13] R. J. Downey *et al.*, "Asynchronous stimulation with an electrode array reduces muscle fatigue during FES cycling," in *Proc. Int. Funct. Elect. Stimulat. Soc.*, Banff, AB, Canada, Sep. 2012, pp. 154–157.

[14] A. R. Lind and J. S. Petrofsky, "Isometric tension from rotary stimulation of fast and slow cat muscles," *Muscle Nerve*, vol. 1, no. 3, pp. 213–218, 1978. [Online]. Available: http://dx.doi.org/10.1002/mus.880010306

[15] A. K. Wise, D. L. Morgan, J. E. Gregory, and U. Proske, "Fatigue in mammalian skeletal muscle stimulated under computer control," *J. Appl. Physiol.*, vol. 90, no. 1, pp. 189–197, 2001. [Online]. Available: http://jap.physiology.org/content/90/1/189.abstract

[16] N. M. Malešević, L. Z. Popović, L. Schwirtlich, and D. B. Popović, "Distributed low-frequency functional electrical stimulation delays muscle fatigue compared to conventional stimulation," *Muscle Nerve*, vol. 42, no. 4, pp. 556–562, 2010. [Online]. Available: http://dx.doi.org/10.1002/mus.21736

[17] T. I. Brown, Y. Huang, D. L. Morgan, U. Proske, and A. Wise, "A new strategy for controlling the level of activation in artificially stimulated muscle," *IEEE Trans. Rehabil. Eng.*, vol. 7, no. 2, pp. 167–173, Jun. 1999.

[18] L. Z. P. Maneski, N. M. Malešević, A. M. Savić, T. Keller, and D. B. Popović, "Surface-distributed low-frequency asynchronous stimulation delays fatigue of stimulated muscles," *Muscle Nerve*, vol. 48, no. 6, pp. 930–937, 2013. [Online]. Available: http://dx.doi.org/10.1002/mus.23840

[19] A. C. Hughes, L. Guo, and S. P. DeWeerth, "Interleaved multichannel epimysial stimulation for eliciting smooth contraction of muscle with reduced fatigue," in *Proc. Annu. Int. Conf. IEEE Eng. Med. Biol. Soc. (EMBC)*, Buenos Aires, Argentina, Sep. 2010, pp. 6226–6229.

[20] K. Yoshida and K. Horch, "Reduced fatigue in electrically stimulated muscle using dual channel intrafascicular electrodes with interleaved stimulation," *Ann. Biomed. Eng.*, vol. 21, no. 6, pp. 709–714, 1993. [Online]. Available: http://dx.doi.org/10.1007/BF02368649

[21] D. McDonnall, G. A. Clark, and R. A. Normann, "Interleaved, multisite electrical stimulation of cat sciatic nerve produces fatigue-resistant, ripple-free motor responses," *IEEE Trans. Neural Syst. Rehabil. Eng.*, vol. 12, no. 2, pp. 208–215, Jun. 2004.

[22] M. Thomsen and P. H. Veltink, "Influence of synchronous and sequential stimulation on muscle fatigue," *Med. Biol. Eng. Comput.*, vol. 35, no. 3, pp. 186–192, 1997. [Online]. Available: http://dx.doi.org/10.1007/BF02530036

[23] R. Nguyen, K. Masani, S. Micera, M. Morari, and M. R. Popovic, "Spatially distributed sequential stimulation reduces fatigue in paralyzed triceps surae muscles: A case study," *Artif. Organs.*, vol. 35, no. 12, pp. 1174–1180, 2011. [Online]. Available: http://dx.doi.org/10.1111/j.1525-1594.2010.01195.x

[24] D. G. Sayenko, R. Nguyen, M. R. Popovic, and K. Masani, "Reducing muscle fatigue during transcutaneous neuromuscular electrical stimulation by spatially and sequentially distributing electrical stimulation sources," *Eur. J. Appl. Physiol.*, vol. 114, no. 4, pp. 793–804, 2014. [Online]. Available: http://dx.doi.org/10.1007/s00421-013-2807-4

[25] L. Z. Popović and N. M. Malešević, "Muscle fatigue of quadriceps in paraplegics: Comparison between single vs. multi-pad electrode surface stimulation," in *Proc. Annu. Int. Conf. IEEE Eng. Med. Biol. Soc. (EMBC)*, Minneapolis, MN, USA, Sep. 2009, pp. 6785–6788.

[26] V. K. Mushahwar and K. W. Horch, "Proposed specifications for a lumbar spinal cord electrode array for control of lower extremities in paraplegia," *IEEE Trans. Rehabil. Eng.*, vol. 5, no. 3, pp. 237–243, Sep. 1997.

[27] B. Lau, L. Guevremont, and V. K. Mushahwar, "Strategies for generating prolonged functional standing using intramuscular stimulation or intraspinal microstimulation," *IEEE Trans. Neural Syst. Rehabil. Eng.*, vol. 15, no. 2, pp. 273–285, Jun. 2007.

[28] R. J. Downey, M. J. Bellman, H. Kawai, C. M. Gregory, and W. E. Dixon, "Comparing the induced muscle fatigue between asynchronous and synchronous electrical stimulation in able-bodied and spinal cord injured populations," *IEEE Trans. Neural Syst. Rehabil. Eng.*, vol. 23, no. 6, pp. 964–972, Nov. 2015.

[29] R. A. Normann *et al.*, "Coordinated, multi-joint, fatigue-resistant feline stance produced with intrafascicular hind limb nerve stimulation," *J. Neural Eng.*, vol. 9, no. 2, pp. 1–13, 2012. [Online]. Available: http://stacks.iop.org/1741-2552/9/i=2/a=026019

[30] N. Sharma, K. Stegath, C. M. Gregory, and W. E. Dixon, "Nonlinear neuromuscular electrical stimulation tracking control of a human limb," *IEEE Trans. Neural Syst. Rehabil. Eng.*, vol. 17, no. 6, pp. 576–584, Dec. 2009.

[31] N. Sharma, C. M. Gregory, M. Johnson, and W. E. Dixon, "Closed-loop neural network-based NMES control for human limb tracking," *IEEE Trans. Control Syst. Technol.*, vol. 20, no. 3, pp. 712–725, May 2012.

[32] C. Freeman *et al.*, "FES based rehabilitation of the upper limb using input/output linearization and ILC," in *Proc. Amer. Control Conf.*, Montreal, QC, Canada, Jun. 2012, pp. 4825–4830.

[33] H. Kawai, M. J. Bellman, R. J. Downey, and W. E. Dixon, "Tracking control for FES-cycling based on force direction efficiency with antagonistic bi-articular muscles," in *Proc. Amer. Control Conf.*, Portland, OR, USA, 2014, pp. 5484–5489.

[34] Q. Wang, N. Sharma, M. Johnson, C. M. Gregory, and W. E. Dixon, "Adaptive inverse optimal neuromuscular electrical stimulation," *IEEE Trans. Cybern.*, vol. 43, no. 6, pp. 1710–1718, Dec. 2013.

[35] T. H. Cheng *et al.*, "Identification-based closed-loop NMES limb tracking with amplitude-modulated control input," *IEEE Trans. Cybern.*, to be published, doi: 10.1109/TCYB.2015.2453402.

[36] M. A. Frankel *et al.*, "Multiple-input single-output closed-loop isometric force control using asynchronous intrafascicular multi-electrode stimulation," *IEEE Trans. Neural Syst. Rehabil. Eng.*, vol. 19, no. 3, pp. 325–332, Jun. 2011.

[37] R. J. Downey, T.-H. Cheng, M. J. Bellman, and W. E. Dixon, "Closed-loop asynchronous neuromuscular electrical stimulation prolongs functional movements in the lower body," *IEEE Trans. Neural Syst. Rehabil. Eng.*, vol. 23, no. 6, pp. 1117–1127, Nov. 2015.

[38] R. J. Downey, T.-H. Cheng, M. J. Bellman, and W. E. Dixon, "Switched tracking control of a human limb during asynchronous neuromuscular electrical stimulation," in *Proc. Amer. Control Conf.*, Chicago, IL, USA, 2015, pp. 4504–4508.

[39] J. L. Krevolin, M. G. Pandy, and J. C. Pearce, "Moment arm of the patellar tendon in the human knee," *J. Biomech.*, vol. 37, no. 5, pp. 785–788, 2004.

[40] T. Watanabe, R. Futami, N. Hoshimiya, and Y. Handa, "An approach to a muscle model with a stimulus frequency-force relationship for FES applications," *IEEE Trans. Rehabil. Eng.*, vol. 7, no. 1, pp. 12–18, Mar. 1999.

[41] R. Kamalapurkar, J. A. Rosenfeld, J. Klotz, R. J. Downey, and W. E. Dixon, "Supporting lemmas for RISE-based control methods," arXiv:1306.3432, 2014. [Online]. Available: http://arxiv.org/abs/1306.3432

[42] M. J. Bellman, T.-H. Cheng, R. J. Downey, and W. E. Dixon, "Cadence control of stationary cycling induced by switched functional electrical stimulation control," in *Proc. IEEE Conf. Decis. Control*, Los Angeles, CA, USA, 2014, pp. 6260–6265.

[43] K. Kiguchi and Y. Hayashi, "An EMG-based control for an upper-limb power-assist exoskeleton robot," *IEEE Trans. Syst., Man, Cybern. B, Cybern.*, vol. 42, no. 4, pp. 1064–1071, Aug. 2012.

[44] W. Yu and J. Rosen, "Neural PID control of robot manipulators with application to an upper limb exoskeleton," *IEEE Trans. Cybern.*, vol. 43, no. 2, pp. 673–684, Apr. 2013.

[45] K. Kiguchi, S. Kariya, K. Watanabe, K. Izumi, and T. Fukuda, "An exoskeletal robot for human elbow motion support-sensor fusion, adaptation, and control," *IEEE Trans. Syst., Man, Cybern. B, Cybern.*, vol. 31, no. 3, pp. 353–361, Jun. 2001.

[46] S. Hussain, S. Q. Xie, and P. K. Jamwal, "Adaptive impedance control of a robotic orthosis for gait rehabilitation," *IEEE Trans. Cybern.*, vol. 43, no. 3, pp. 1025–1034, Jun. 2013.

[47] B. E. Paden and S. S. Sastry, "A calculus for computing Filippov's differential inclusion with application to the variable structure control of robot manipulators," *IEEE Trans. Circuits Syst.*, vol. 34, no. 1, pp. 73–82, Jan. 1987.

[48] N. Fischer, R. Kamalapurkar, and W. E. Dixon, "LaSalle–Yoshizawa corollaries for nonsmooth systems," *IEEE Trans. Autom. Control*, vol. 58, no. 9, pp. 2333–2338, Sep. 2013.

Ryan J. Downey received the B.S. degree in mechanical engineering from the University of Florida, Gainesville, FL, USA, in 2010, where he participated in a Research Experiences for Undergraduates Program, the first M.S. degree in biomedical engineering from Politecnico di Milano, Milan, Italy, in 2012, the second M.S. degree in biomedical engineering, and the third M.S. and Ph.D. degrees in mechanical engineering from the University of Florida, in 2012, 2014, and 2015, respectively.

He joined the Nonlinear Controls and Robotics Group with the University of Florida as an undergraduate researcher in 2009 and subsequently began his doctoral studies in 2010. In 2011, he was accepted to an International Exchange Program (ATLANTIS CRISP) with Politecnico di Milano. He is currently a Post-Doctoral Scholar with the Medical University of South Carolina. His current research interests include functional electrical stimulation, Lyapunov-based nonlinear control, stroke, and sensory stimulation.

Dr. Downey was a recipient of the 2015 American Automatic Control Council O. Hugo Schuck (Best Paper) Award.

Teng-Hu Cheng received the B.S. and M.S. degrees in mechanical engineering from National Taiwan University, Taipei, Taiwan, in 2007 and 2009, respectively, and the Ph.D. degree in mechanical engineering from the University of Florida, Gainesville, FL, USA, in 2015.

He joined the Nonlinear Controls and Robotics Group with the University of Florida, as a Doctoral Student under the advisement of Dr. W. Dixon in 2011. In 2013 and 2014, he was a Research Intern with the Air Force Research Laboratory, Eglin Air Force Base, FL, USA, and the University of Florida Research and Engineering Education Facility, Shalimar, FL, USA, aiding in designing cooperative control for networked systems with time-varying network topologies and developing event-driven control for networked systems. In 2015, he was a perceptual computing Software Intern in IoTG with Intel, Santa Clara, CA, USA, for seven months. His current research interests include networked system control, switched control, event-driven control, and nonlinear control.

Dr. Cheng was a recipient of the 2015 American Automatic Control Council O. Hugo Schuck (Best Paper) Award.

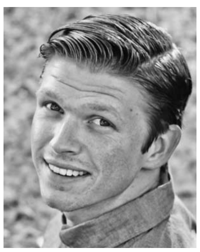

Matthew J. Bellman received the bachelor's and master's degrees, *magna cum laude*, in mechanical engineering with a minor in biomechanics from the University of Florida, Gainesville, FL, USA, and the doctoral degree in mechanical engineering from the University of Florida as a National Defense Science and Engineering Graduate Fellow (NDSEG), focussing on the theoretical development of robust, adaptive control systems for applications involving functional electrical stimulation, specifically those involving rehabilitation and mobility of the lower extremities.

He has been a Member of the Nonlinear Controls and Robotics Group since 2009.

Dr. Bellman was a recipient of the 2015 American Automatic Control Council O. Hugo Schuck (Best Paper) Award.

Warren E. Dixon (M'94–F'16) received the Ph.D. degree from the Department of Electrical and Computer Engineering, Clemson University, Clemson, SC, USA, in 2000.

He was a Eugene P. Wigner Fellow with Oak Ridge National Laboratory (ORNL), Oak Ridge, TN, USA. In 2004, he joined the University of Florida, Gainesville, FL, USA, with the Mechanical and Aerospace Engineering Department, where he currently holds the Newton C. Ebaugh Professorship. He has published three books, an edited collection, 12 chapters, and over 100 journal and 200 conference papers. His current research interest include the development and application of Lyapunov-based control techniques for uncertain nonlinear systems.

Dr. Dixon was a recipient of the 2009 and 2015 American Automatic Control Council O. Hugo Schuck (Best Paper) Award, the 2013 Fred Ellersick Award for Best Overall MILCOM Paper, the 2012–2013 University of Florida College of Engineering Doctoral Dissertation Mentoring Award, the 2011 American Society of Mechanical Engineers Dynamics Systems and Control Division Outstanding Young Investigator Award, the 2006 IEEE Robotics and Automation Society Early Academic Career Award, the National Science Foundation CAREER Award from 2006 to 2011, the 2004 Department of Energy Outstanding Mentor Award, and the 2001 ORNL Early Career Award for Engineering Achievement. He is an IEEE Control Systems Society Distinguished Lecturer.